Memory effect, defect density wave, and related microdomain structure in an incommensurate phase of barium sodium niobate

S. Mori and N. Yamamoto
Department of Physics, Tokyo Institute of Technology, Meguro-ku, Tokyo 152, Japan

Y. Koyama
Kagami Memorial Laboratory for Materials Science and Technology, and Advanced Research Center for Science and Engineering, Waseda University, Shinjuku-ku, Tokyo 169, Japan

Y. Uesu
Advanced Research Center for Science and Engineering, and Department of Physics, Waseda University, Shinjuku-ku, Tokyo 169, Japan
(Received 22 June 1994)

A microstructure causing the memory effect in the incommensurate phase of barium sodium niobate was investigated by means of a transmission electron microscope. A type of microdomain structure, which is constituted of a complicated array of microscopic ferroelastic domains with a modulation along the [100] direction, is found. Because this microdomain structure appears reversibly during the heating and cooling processes, the microdomain structure is directly related to the memory effect.

A memory effect in incommensurate phases has been investigated, so far, in insulating materials such as Rb_2ZnCl_4 and $Ba_2NaNb_5O_{15}$ and some charge-density-wave compounds such as TaS_3.[1-3] The memory effect is characterized by the fact that, after a sample is maintained for an adequate amount of time at an annealing temperature (T_A) within the incommensurate phase, the sample exhibits different physical properties from those in a nonannealed sample. The most remarkable property of the memory effect is that an incommensurate wave vector is unchangeable in several degrees around T_A in heating and subsequent cooling processes.

Among the above materials, barium sodium niobate, $Ba_2NaNb_5O_{15}$ (BSN), is known to exhibit the most conspicuous memory effect. The effect in BSN is understood to be related to a phase transition from a tetragonal phase (space group; $I4mm$) to an incommensurate one in a cooling process at 573 K. Kiat, Calvarin, and Schneck show that in a sample, which is kept at T_A for several days and subsequently quenched to room temperature, a satellite reflection characterizing the incommensurate structure is split into two reflection spots on cooling from T_A.[4-6] It is suggested that this splitting is due to the coexistence of two states, the $1q$ and $2q$ states.[5-7] The $1q$ state is characterized by a modulation along only the $[100]_o$ direction and the $2q$ state by the modulation along both the $[100]_o$ and $[010]_o$ directions. Note that a suffix o denotes an orthorhombic system. Manolikas *et al.* showed from transmission-electron-microscope observation that two distinct regions with different density of discommensurations exist in an annealed sample at room temperature.[7] One is characterized as a low-density region of discommensurations (LDR) near a ferroelastic domain wall and the other is a high-density region of discommensurations (HDR) in a ferroelastic domain.[7-8] It was also pointed out that the state associated with the LDR is the $2q$ state, while the state with the HDR is the $1q$ one.[7] It is hence understood that the coexistence of these two distinct regions in the annealed sample is closely related to the splitting of a satellite reflection. In addition, it is recently revealed from the x-ray-diffraction, birefringence, and optical experiments that the $2q$ state has a tetragonal symmetry macroscopically and the $1q$ state has an orthorhombic one.[6-9] However, the details of the two states in the sample exhibiting the memory effect have not been sufficiently understood so far.

A recent explanation of the memory effect in the incommensurate phases of the insulating materials is made on the assumption of the existence of a defect density wave (DDW).[2,5,10] That is, an interaction between mobile defects included in a sample and an incommensurate modulation gives rise to an ordered pattern of defects; the DDW. In the case of BSN, the DDW should be due to Na mobile ions. Then, the ordered pattern causes the appearance of physical properties characterized as the memory effect, which was mentioned earlier. However, a correlation between the DDW and the coexisting two states remains unsolved.

In this paper we describe the details of microstructures causing the memory effect in the incommensurate phase of BSN, which were observed by means of a transmission-electron microscope. Then, we show a microdomain structure characterizing the memory effect on the basis of an analysis of experimental results. Moreover, features of the memory effect such as the DDW are discussed in relation to the microdomain structure found in the present work.

A (001) plate of a BSN single crystal was prepared by polishing mechanically down to 50 μm and subsequently thinned by an Ar ion beam. A thermal treatment to produce the memory effect was made in the following. In order to erase the previous hysteresis, first of all, a sample was annealed at 723 K within the high-temperature tetragonal phase for 24 h. In the present work, the sam-

ple annealed only at 723 K is called a *nonannealed* sample. For an *annealed* sample, the sample was further annealed at T_A of 533 K within the incommensurate phase for 72 h and then cooled rapidly down to room temperature. The observation was made using JEM-200CX equipped with a double-tilted heating holder. A microstructure related to the memory effect was mainly observed by satellite dark-field images using incommensurate satellite reflections. Here, let us briefly describe a condition under which satellite dark-field images are taken in the present work. Figure 1 shows a part of a reciprocal lattice of the incommensurate phase in BSN. Since BSN consists of a twin structure due to the lowering of the symmetry, a fundamental spot of the high-temperature tetragonal structure is split into two reflection spots of the orthorhombic structure and incommensurate satellite spots also appear at positions indicated by arrows (α) and (β). That is, satellite spots are, respectively, due to one of the $1q$ ferroelastic domain of the twin structure and the other domain. Note that the splitting of the fundamental spots is not, for simplicity, depicted in Fig. 1. In this paper, satellite spots due to one ferroelastic domain and the other are, generally, called (α)- and (β)-type spots, respectively. Thus, three different kinds of satellite dark-field images can be obtained by using each incommensurate satellite spots; that is, the (α)-type spot, the (β)-type spot and both the (α)- and (β)-type spots.

Figure 2 shows satellite dark-field images of BSN obtained at room temperature. Figure 2(a) is an image of the nonannealed sample, taken by both the (α)- and (β)-type spots, while images of the annealed sample by using the (α)-type spot and the (β)-type one are shown in Figs. 2(b) and 2(c), respectively. As is shown in Fig. 2(a), in the case of the use of both the (α)- and (β)-type spots, very wavy black line contrasts are observed in each ferroelastic domain of the nonannealed sample, in addition to a white line contrast due to the ferroelastic domain wall parallel to the $(110)_o$ plane, which is indicated by an arrow. It should be noticed that, because the incommensurately modulated direction in the $1q$ domain is the $[100]_o$ direction, a direction of the modulation of one domain in two neighboring domains differs from that in the other by about 90°. As is shown in our previous paper, further, each black line is identified as a discommensuration with a phase slip of $2\pi/4$.[11] On the other hand, the Figs. 2(b) and 2(c), a ferroelastic domain wall is observed as a boundary between the bright and dark contrast regions, as marked by an arrow (A), using either the (α)-type spot or the (β)-type one. Discommensurations are also observed as the wavy black contrasts. The most important part of the images is that a microstructure is found in the large $1q$-ferroelastic domain; that is, in a region marked by an arrow (B). From the contrast reverse in Figs. 2(b) and 2(c), this microstructure is understood to be a microdomain structure consisting of the two $1q$-ferroelastic microdomains. A width of each microdomain is estimated to be about 45 nm. A feature of the microdomain structure is that the boundary between two microdomains is not straight but wavy, in contrast to the ferroelastic domain wall indicated by an arrow (A). It is worth remarking that, although each ferroelastic microdomain is obviously regarded as the $1q$ state from the contrast reverse, the microdomain structure can be, as an average structure, identified as the $2q$ state with the

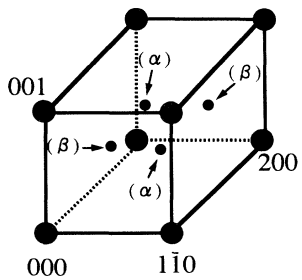

FIG. 1. Reciprocal lattice of the incommensurate phase of BSN. Large and small circles denote fundamental and incommensurate satellite spots, respectively.

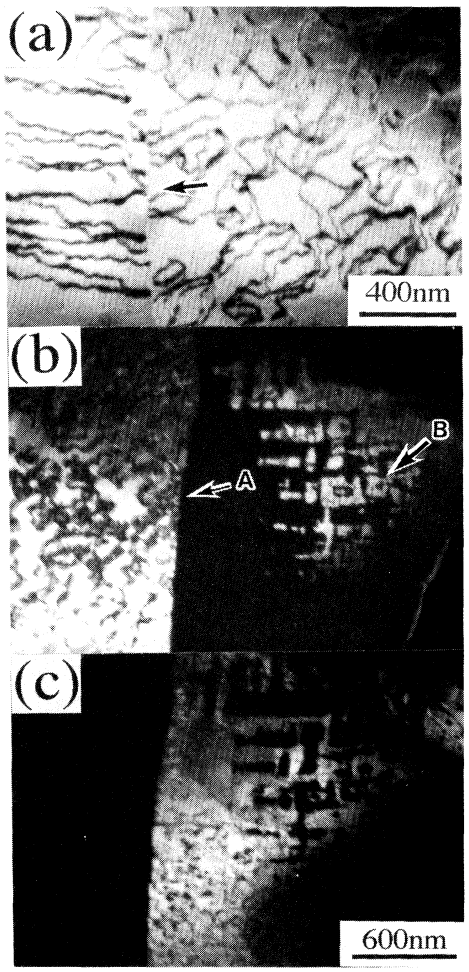

FIG. 2. Satellite dark-field images obtained at room temperature from a *nonannealed* sample (a), and an *annealed* sample, (b) and (c). The image (a) was taken by both (α)- and (β)-type satellite reflections in Fig. 1. On the other hand, the images (b) and (c) were obtained by only the (α)-type spot and only the (β)-type one, respectively.

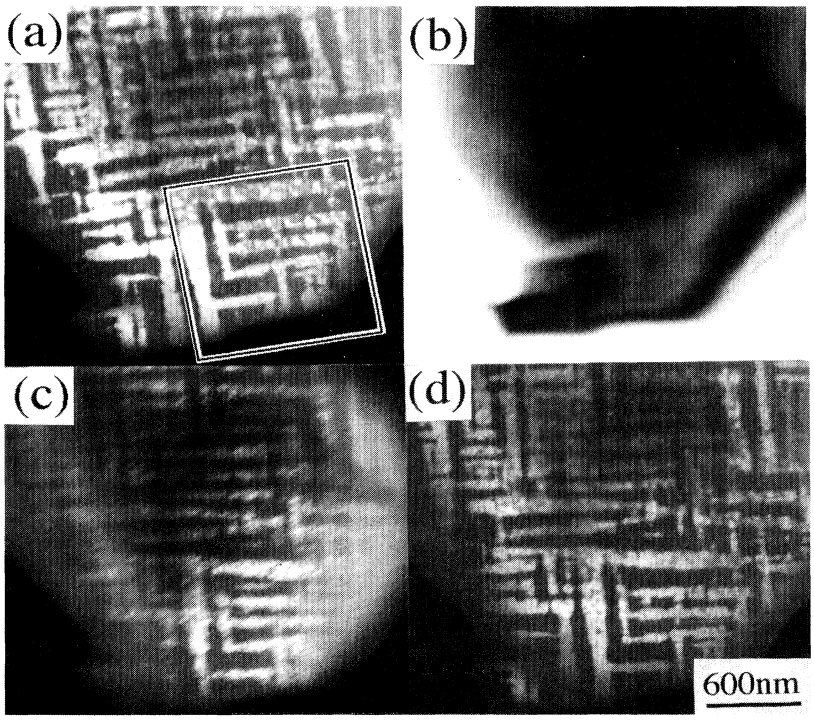

FIG. 3. Change in microstructure during the heating and subsequent cooling processes. The images (a), (c), and (d), are satellite dark-field images taken, by using only a (α)-type spot, at (a) room temperature before heating, (c) 513 K during cooling and (d) room temperature after cooling, respectively. Because of no satellite reflections in the high-temperature tetragonal phase, the image (b) is a bright-field image taken at 623 K.

modulation along both the $[100]_o$ and $[010]_o$ directions because of the small size of each microdomain.

In order to investigate a correlation between the memory effect and the microdomain structure, *in situ* observation of the tetragonal-to-incommensurate transition was carried out. Figure 3 shows a sequence of the change in microdomain structure of the annealed sample, which was observed during the process of heating to the high-temperature tetragonal phase and subsequently cooling to room temperature. Figure 3(a) is a satellite dark-field image taken at room temperature. Note that satellite dark-field images shown in this figure were taken by using only the (α)-type spot. In the image, both a microdomain contrast and black line contrast identified as a discommensuration are clearly seen. When the temperature is raised from room temperature, the contrast due to a microdomain structure becomes faint and then is invisible around 573 K. As is shown in Fig. 3(b), no contrast is observed in a bright-field image taken at 623 K. Note that on heating BSN undergoes the phase transition from the incommensurate phase to the high-temperature tetragonal phase around 573 K. On the other hand, when the temperature is lowered from the high-temperature tetragonal phase, a faint contrast of the microdomain structure appears around T_A of 533 K again. At the same time, an intensity of the satellite reflection increases rapidly. As is seen in Fig. 3(c), the faint contrast due to a microdomain structure is actually observed in the satellite dark-field image at 513 K. In addition, the discommensuration can be detected as a driftlike contrast of the sample. Because an edge of the sample is seen sharply, the driftlike contrast is a real contrast due to the discommensuration line. Then, the discommensuration line at 513 K is understood to be very diffuse. On further cooling to room temperature, the contrast due to the microdomain structure is slightly developed, as shown in Fig. 3(d). From a comparison between Figs. 3(a) and 3(d), it is understood that the microstructure after the heating and subsequent cooling processes is identical to the initial structure in Fig. 3(a). That is, the microdomain structure appears reversibly in the heating and subsequent cooling processes. In addition to the reversibility of the microdomain structure, the fact that the microdomain contrast appears around T_A of 533 K also suggests that the microdomain structure has a direct relation to the memory effect in the incommensurate phase of BSN.

The details of the microdomain structure was concretely analyzed from both diffracion patterns and satellite dark-field images. We actually analyzed several microdomain contrasts in different regions of the annealed sample. As an example, the result of a rectangle part of the microdomain in Fig. 3(a) is schematically depicted in Fig. 4. From Fig. 4, the microdomain structure is under-

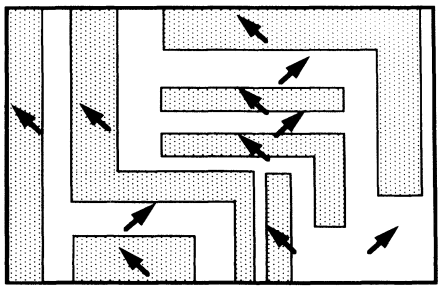

FIG. 4. Analysis of a rectangle part of the microdomain structure shown in Fig. 3(a). An arrow denotes the $[100]_o$ direction in each ferroelastic microdomain, which is a direction of the incommensurate modulation.

stood to consist of a complicated array of the ferroelastic domains with a width of about 45 nm. Note that in each microscopic ferroelastic domains the modulation has an incommensurate period along only the $[100]_o$ direction. Domain boundaries are basically perpendicular to the $\langle 110 \rangle_o$ directions although the boundary is very wavy and diffuse. It is worth noticing that the microdomain structure found in the present work is consistent with the domain structure of the $2q$ state, which was speculated by Barre, Mutka, and Roucau.[8] In other words, the microdomain structure obtained here is direct evidence of the $2q$ incommensurate structure of BSN, and the $1q$ and $2q$ states are understood to coexist in the incommensurate phase. The splitting of the satellite reflection, which was found by Kiat, Calvarin, and Schneck,[4-6] is experimentally concluded to be due to the coexistence of the $1q$ and $2q$ states.

We now discuss an origin of the memory effect in relation to the microdomain structure. Among the present experimental data, we pay an attention to the fact that the domain boundary in the microdomain structure is not straight, but wavy and diffuse. It is obvious that the wavy and diffuse boundary produces a strain field and is energetically unstable. Then a relaxation process should occur in the annealing in order to release the strain energy. In the case of BSN, there is a Na ion as a mobile ion in a sample. So, the strain energy can be released by the redistribution of the Na mobile ions. The Na mobile ions would move toward the microdomain boundary, so that they produce an ordered pattern along the boundary. This is a reason why the wavy and diffuse boundary is stabilized in the real sample. Note that the array of the Na mobile ions along the boundary is definitely identified as the DDW proposed for the memory effect.[2,4-8,10] The formation of the DDW is then understood to result from the relaxation of the strain field produced by the wavy and diffuse microdomain boundary.

Eventually, we propose the following scenario of the memory effect. In the annealed sample cooled from T_A, there exists the microdomain structure with the distribution of the Na ions along the microdomain boundary in the large $1q$ ferroelastic domain. When the temperature is raised to the high-temperature tetragonal phase, the microdomain structure disappears at the transition temperature of the reverse transition but the Na distribution still remains. The remaining distribution produces a strain field in the high-temperature tetragonal phase and the Na ions should diffuse in order to release the strain energy. Because of a large relaxation time of the Na diffusion, the distribution of the Na ions is not effectively changed for a short time. In this situation, when the temperature is lowered to the incommensurate phase, the microdomain appears with a boundary along the Na distribution in order to release the strain energy. In addition, the Na ions should pin the discommensuration line. As a result of the pinning, the incommensurability does not change in several tens of degrees around T_A.

In the present work we found a microdomain structure causing the memory effect. This microdomain structure is constituted of the complicated array of microscopic ferroelastic domains with the modulation along the $[100]_o$ direction and can be identified as the $2q$ incommensurate structure in an average structure. In addition, the DDW of the Na mobile ions should form in order to release the strain energy produced by the wavy and diffuse microdomain boundary.

[1]H. G. Unruh, J. Phys. C **16**, 3245 (1983).
[2]J. C. Toledano, J. Schneck, and G. Errandonea, in *Incommensurate Phases in Dielectric,* edited by R. Blinc and A. P. Levanuyk (Elsevier, Amsterdam, 1985), Vol. 14, Pt. 2, p. 233.
[3]G. Mihaly and L. Mihaly, Solid State Commun. **48**, 449 (1983).
[4]J. M. Kiat, G. Calvarin, and J. Schneck, Jpn. J. Appl. Phys. Suppl. **24-2**, 832 (1985).
[5]J. M. Kiat, G. Calvarin, and J. Schneck, Ferroelectrics **105**, 219 (1990).
[6]J. M. Kiat, G. Calvarin, and J. Schneck, Phys. Rev. B **49**, 776 (1994).
[7]C. Manolikas, J. Schneck, J. C. Toledano, J. M. Kiat, and G. Calvarin, Phys. Rev. B **35**, 8884 (1987).
[8]S. Barre, H. Mutka, and C. Roucau, Phys. Rev. B **38**, 9113 (1988).
[9]J. M. Kiat, Y. Uesu, M. Akutsu, and J. Aubree, Ferroelectrics **125**, 227 (1992).
[10]G. Errandonea and J. Schneck, Jpn. J. Appl. Phys. Suppl. **24-2**, 847 (1985).
[11]S. Mori, Y. Koyama, and Y. Uesu, Phys. Rev. B **49**, 621 (1994).

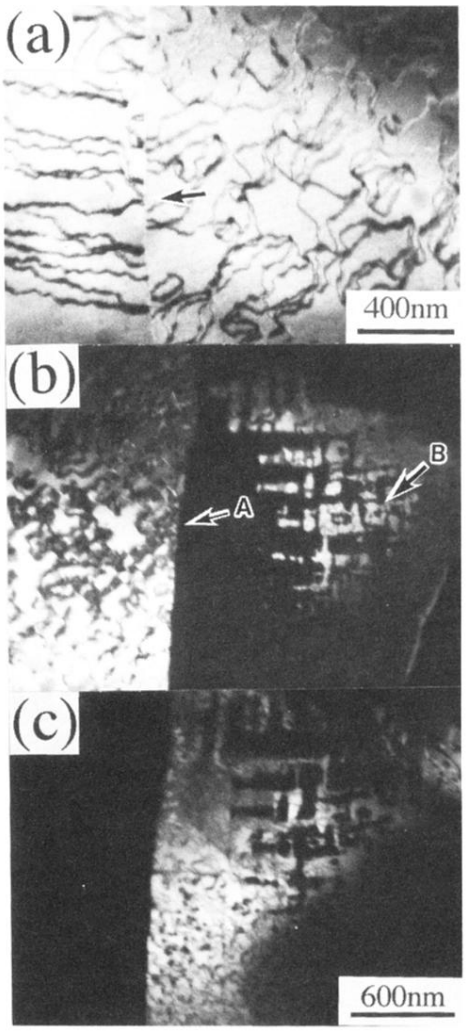

FIG. 2. Satellite dark-field images obtained at room temperature from a *nonannealed* sample (a), and an *annealed* sample, (b) and (c). The image (a) was taken by both (α)- and (β)-type satellite reflections in Fig. 1. On the other hand, the images (b) and (c) were obtained by only the (α)-type spot and only the (β)-type one, respectively.

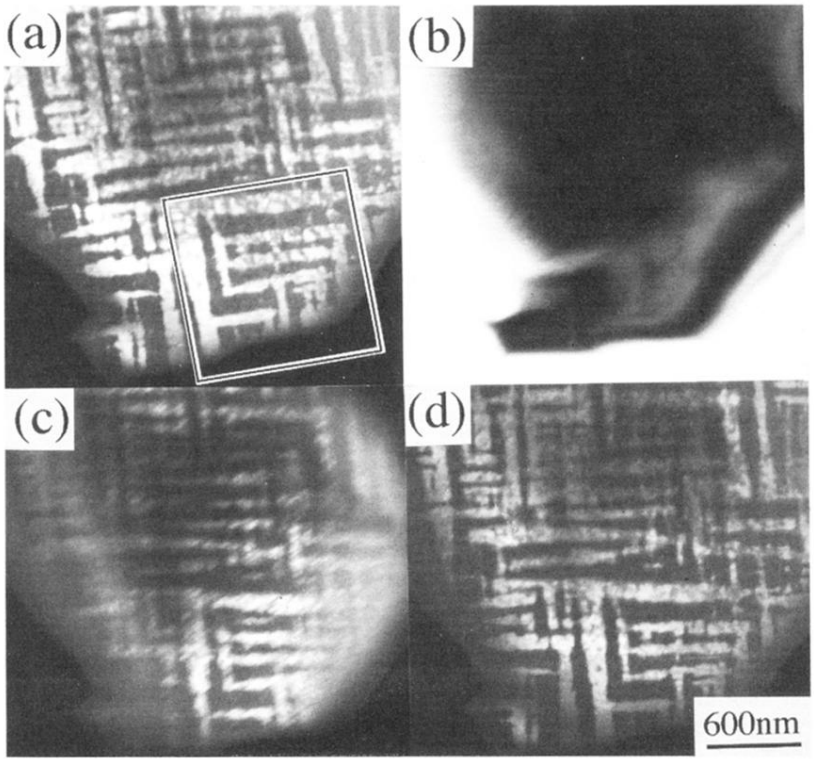

FIG. 3. Change in microstructure during the heating and subsequent cooling processes. The images (a), (c), and (d), are satellite dark-field images taken, by using only a (α)-type spot, at (a) room temperature before heating, (c) 513 K during cooling and (d) room temperature after cooling, respectively. Because of no satellite reflections in the high-temperature tetragonal phase, the image (b) is a bright-field image taken at 623 K.